

KINEMATIC TIME MIGRATION/DEMIGRATION: AUTOMATIC VELOCITY MODEL BUILDING AND MIGRATION DECONVOLUTION

M. Glöckner, S. Dell, B. Schwarz, C. Vanelle, and D. Gajewski

email: *martina.gloeckner@uni-hamburg.de*

keywords: *Demigration, VMB, deconvolution*

ABSTRACT

To obtain an image of the earth's subsurface, time-domain methods can be applied at the first step as they are very fast, less sensitive to the model errors than depth-domain methods and, usually, massively parallelized techniques. A powerful tool for time imaging consists of a series of time migration and demigration with a subsequent stacking. Demigration describes the process of data prediction by a given reflectivity model and is an inverse to migration. Migration is a back transformation process which maps seismic data to reflectivity model, respectively. The advantage of these data domain transformations are data regularisation, illumination compensation and amplitude recovering. Apart of the data enhancement, the transformations incorporate an intrinsic handling of conflicting dips. Furthermore, the time demigration allows a velocity model building (time-migration velocities) in a automatic data-driven fashion. The model building implicates a coherence filtering of the migration velocities which comprises a thresholding followed by velocities interpolation and smoothing. This implies that not only prominent reflections but also weaker diffractions are enhanced. Moreover migration/demigration duality allows to formulate the time migration in a least-squares fashion. We directly approximate the inverse of the Hessian which allows us to perform one-iteration least-squares migration, or migration deconvolution, respectively. Also here, we do not use any model assumptions and approximate the Hessian inverse by nonstationary matching filters, i.e., in an automated fashion. Therefore, a minimal user interaction is required to carry out both the model and image update. To validate our time-imaging method, we applied it to complex field data examples including complex salt intrusions and diagonal faulting.

INTRODUCTION

Time migration is an attractive tool to produce subsurface images because it is very fast, less sensitive to model errors than depth migration and, usually, massively parallelized technique. A highly focused time image is however only achievable with well determined migration velocity models. Thus, a refinement of the initial time-migration velocities is often applied to obtain an improved final image. Also the time-migration operator is derived by considering many assumptions, among others a straight (bended) ray propagation, regularly sampled seismic data and infinite migration aperture. These assumption are hardly to fulfil when processing field data. Thus, time-migrated images usually suffer from the imperfections of the operator exhibiting several artifacts (see, e.g., in Hertweck et al., 2003), among others well-known migration swings. Conventionally, a residual moveout (RMO) analysis is used to reduce the impact of the model errors on the image. The RMO analysis is an iterative approach based on the analysis of the RMO of time-migrated events in common-image gathers (CIG). Another approach to perform the velocity update after prestack time migration is common-offset migration followed by restoration of inverse normal moveout (NMO) and subsequent velocity analysis on the newly generated gathers. The obtained gathers

contain time-migrated reflections with a hyperbolic moveout and are therefore very suitable for classical one-dimensional or a multi-dimensional velocity analysis (see, e.g., in Dell et al., 2012). To reduce migration artifacts, several image-enhancement techniques, e.g., dip or structure-oriented filter, are usually applied posterior time migration. These methods however introduce a certain smoothing into migrated images, which may increase uncertainties in the fault interpretation.

We propose a unique technique to tackle both time-migration problems mentioned above. The method is based on the duality of modelling/imaging operators (see in Claerbout et al., 1996). On the one hand, time-migration is a hyperbola summation (amplitude stacking) which aims to focus events, corrects dips, and collapses diffractions. On the other hand, time-demigration is a semicircle superposition (amplitude spreading) which aims to restore (model) seismic data based on provided reflectivity models. A comprehensive imaging theory based on migration and demigration is presented in (Hubral et al., 1996; Tygel et al., 1996). Huygens's surfaces and isochrons are used as most basic concept and are combined with dynamic methods. While the main focus in those papers is on depth imaging, Iversen et al. (2012) presented a time-based approach. They used reflection times, curvatures, and slopes as parameters to perform migration and demigration. The advantage of the forward and backward transformation is data enhancement and regularisation due to incorporated summation. Furthermore, a general conflicting dip handling is naturally implied by the migration process. On the one hand, a correct migrated image should not contain conflicting dips with the exception of multiples. On the other hand, the demigration reconstructs the dips in the original domain. A precondition to perform these steps is a suitable velocity model, which can be automatically generated via the common-reflection-surface (CRS) method (Jäger et al., 2001).

In the first part of the paper, we present a data-driven demigration approach. We then explain our method to update the migration velocities. The method utilises the kinematic wavefield attributes (see in Hubral, 1983) and also comprises a coherence filtering of the velocities which further improves the final models. In the second part, we briefly review the theory of the least-squares migration and show that time migration/demigration operators could also be used for migration deconvolution. The application to complex marine data examples completes this paper.

PART I: AUTOMATIC VELOCITY MODEL BUILDING

Generally, geophysical modeling uses linear operators that predict data from models (Claerbout et al., 1996). The inverse of the modeling, seismic inversion, aims to find models from the data and also uses linear operators. The modeling operators with respect to reflectivity are conventionally referred to as demigration operators. Their inverse operators are referred to as migration operators. In our paper, we formulate time migration and demigration operator based on a higher-order paraxial traveltimes approximation. We suggest to use the implicit CRS operator (Schwarz et al., 2014) as it belongs to the double-square-root (DSR) operator family. In principle, any DSR operator (see in Walda et al., 2017) can be used instead of implicit CRS. First, we apply implicit CRS operator to prestack data in order to extract kinematic wavefield attributes. The initial time-migration velocities are then calculated using the extracted attributes. As implicit CRS operator is a stacking operator, i.e., it is parametrized by the two-wave traveltimes along the central zero-offset ray, we reformulate it to the time migration operator by rewriting the operator in apex coordinates. The re-parametrized implicit CRS operator reads:

$$t = \sqrt{\frac{t_{apex}^2}{4} + \frac{(\Delta x_a - h)^2}{V^2}} + \sqrt{\frac{t_{apex}^2}{4} + \frac{(\Delta x_a + h)^2}{V^2}}, \quad (1)$$

where $\Delta x_a = x_m - x_{apex}$ is the midpoint displacement, h is the half-offset, V denotes the time migration velocity and t_{apex} is the apex travel time (Bobsin, 2014). This double-square-root expression 1 resembles a conventional Kirchhoff time migration operator (Yilmaz and Claerbout, 1980). The migration velocity V is expressed through the kinematic wavefield attributes (Schwarz et al., 2014) as

$$V = \frac{v_{NMO}}{\sqrt{1 + \frac{v_{NMO}^2}{v_0^2} \sin^2 \alpha}} \quad \text{where} \quad v_{NMO} = \sqrt{\frac{2v_0 R_{NIP}}{t_{apex} \cos^2 \alpha}}, \quad (2)$$

where α is the incidence angle and R_{NIP} is the radius of curvature of the normal incidence point (NIP) wave. Equation 2 includes the normal move out (NMO) velocity, v_{NMO} . As we also consider the incidence

angle α , we directly obtain dip-corrected migration velocities. In total, the migration velocity (Equation 2) depends on four parameters: α , R_{NIP} , the considered time t_{apex} , and near-surface velocity v_0 . The near-surface velocity is an important counterpart of the migration velocity and is usually based on a good guess. However, the formulation of migration velocity as in Equation 2 allows a near-surface velocity scan. This appears to be an attractive complementary benefit of Equation 2, particularly for data acquired in regions with very complex near-surface geology, e.g., in desert. As the kinematic wavefield attributes are extracted (guessed) during an automatic implicit CRS stacking, the velocity model building (VMB) is a purely data-driven process with a minimal user interaction.

For the data modeling process, we change the dependency of Equation 1. In Equation 1, the travel time t is a function of apex time t_{apex} and lateral deviation from the apex location Δx_a . To obtain the corresponding demigration expression, we solve Equation 1 for t_{apex} :

$$t_{apex} = \sqrt{t^2 - \frac{4(\Delta x_a^2 + h^2)}{V^2} + \frac{16\Delta x_a^2 h^2}{t^2 V^4}}, \quad (3)$$

which is a single-square-root expression in contrast to the double-square-root formulation of the migration operator. The demigration as well as the migration equations are also valid for the poststack case, where the half offset h vanishes and the equations are simplified.

Finally, we apply a coherence-filtering to migration velocities (Gloeckner et al., 2016). We use the coherence section produced by time-migration and define a certain threshold. All values below the threshold are multiplied with zero and values above are multiplied with one. Then, the weighted coherence section serves as mask for the velocity model and gaps are interpolated. As a result areas with large coherence imply a reliable migration velocity and the subsequent interpolation links these areas to obtain an improved migration velocity model. Furthermore, diffractions are naturally enhanced in the suggested strategy, because diffractions are fitted by the migration operators, whereas reflection events are merely repositioned.

PART II: MIGRATION DECONVOLUTION

As outlined in the first part, we can also formulate migration/demigration operator duality for time imaging. In operator notation it reads:

$$d = Lm, \quad m = L^{-1}d, \quad (4)$$

where d is seismic data, m is the reflectivity model (migration image), L is the linear modeling operator, and L^{-1} is the inverse (migration) operator. Usually, adjoint operators are used in calculations instead of inverse operators as they tolerate imperfections in the data and does not demand that the data provide full information (Claerbout et al., 1996).

The operator duality in Equation 4 allows us to formulate migration as a least-squares problem. If we consider the following functional

$$J(m) = \frac{1}{2} (Lm - d)^2. \quad (5)$$

we immediately see that the gradient $\frac{\partial J}{\partial m}$ yields us the least-squares estimate of the reflectivity model

$$\frac{\partial J}{\partial m} = 0 \implies \hat{m} = (L'L)^{-1}Ld, \quad (6)$$

where we use adjoint operator L' instead of the inverse operator L^{-1} . We also note in Equation 6 the inverse of the Hessian $(L'L)^{-1}$. This inverse is frequently referred in the literature as a deconvolution operator or resolution matrix (see in Hu et al., 2001). We also can use this inverse to perform a deconvolution of the migrated image to correct the amplitudes. Due to the higher-order complexity of the migration operators in the reality, the Hessian cannot generally be inverted, and iterative procedures such as conjugate gradient (CG) or the Newton method are often used (see, e.g., in Lambaré et al., 1992). We use a method suggested in Guitton (2004) to approximate the effects of the Hessian with nonstationary matching filters. Apart of a very handy implementation, the method simulates the effects of least-squares inversion at a much reduced cost than an iterative approach. The used method is summarised in Guitton (2004) as followed:

- Compute a first migrated image $m_1 = L'd$.

- Compute a second image $m_2 = L' L m_1$.
- Estimate a bank of nonstationary matching filters B_0 so that $m_1 = B_0 m_2$.
- Convolve B_0 with m_1 to get an improved image $\hat{m} = B_0 m_1$.

Convolution of the nonstationary matching filters with the first migrated image is equal to so-called one-iteration least-squares migration.

FIELD DATA EXAMPLE

We applied the proposed migration/demigration loop to two marine data examples. The first data set was acquired by TGS in the Levantine basin, Eastern Mediterranean Sea. The Levantine Basin has a complex seismic stratigraphy of the basinal succession. The deformation pattern of the intraevaporitic sequences include folds and thrust faulting, which gives evidence for extensive salt tectonics and shortening during the depositional phase. Postdepositional gravity gliding caused salt rollers in the extensional marginal domain, compressional folds, and faults within the Levantine basin (Netzeband et al., 2006). A subset of the data consisting of around 2000 CMP gathers with a total line length of approximately 15 km, a shot/receiver spacing of 25 m, a CMP spacing of 12.5 m, and maximum offsets of 7325 m was chosen. The maximum CMP fold is about 120 traces. The record length was 8 s with a 4 ms sample rate. Figure 1 shows the automatically generated velocity model on top and the prestack time migrated image on the bottom. Please note that the water column is muted. The velocity model obtained by coherence-filtering and interpolation is smooth and velocities increase with time except for the first ocean bottom multiple, which produces lower velocities at larger times which can be seen between 2 and 3 s in the lower left corner. The white and red colours in the time velocity model indicate higher salt velocities for the triangular structures: the velocity in the sediments is about 2000 *m/s* while in the salt, it is about 4000 *m/s*. Indications of a sedimentary layering are visible in both images. The migrated image shows some faults starting from the triangular structures and originating at the sea floor. The sedimentary layering is horizontally ruptured by a chaotic pattern, which coincides with a slided slump complex (Hübscher and Netzeband, 2007).

Following Hubral et al. (1996), we choose the same apertures and velocity models for forward and backward transformation. The midpoint aperture ranges from 1500 m to 2500 m and the offset aperture from 1000 m to 7000 m. To evaluate the results of the demigration, we compare common offset sections of the original and the demigrated data. Figure 2 shows common offset sections for $h = 500$ m, where the original data is presented on the left and the demigrated data on the right. The demigration enhances the data quality and the events are continuously imaged. The second dipping reflection, starting at 1.8 s, with the diffraction hyperbolas is enhanced. Furthermore, structures below this reflection are better visible in the demigrated section. In addition, the first ocean bottom multiple is more pronounced too but reflections below, which are masked in the original data section, are visible in the demigrated section. This makes us confident, we are able to reconstruct the original data as well as improve the resolution for deeper events in the velocity model.

Figure 3 shows a good resolution of the salt body (between 2.7-2.9 seconds) and the faults above for both migrated images. Note a clearly observable wavelet-tightening in the updated migration result, i.e. deconvolution. Therefore, faults are more sharp and the sedimentary layering is better visible.

Our second data example is acquired in the North Sea close to the German coastline. Salt structures and complex fault systems characterise the region. The sedimentation process started in the Upper Rotliegend and continued to the evaporites of the Zechstein Group, which reached up to 800 m in thickness. Different phases of salt movements that started in Triassic time formed the salt structures of the region. Each phase is characterised by changing tectonic regimes and different kinds of salt diapirism. To test our method, we chose a part of the data consisting of 4000 CMP gathers with a total line length of approximately 26.5 km. Seismic reflection data were acquired in a 2D marine survey. The shotpoint spacing was 25 m. The receiver group spacing was 12.5 m. The acquisition geometry leads to 6.25 m of CMP spacing and a maximum CMP fold of 60. The record length was 7 s with 4 ms sample rate. No well information was available. We also note that the chosen part of the data represents a shallow marine acquisition, i.e., additionally to the complex diapir structures, we face missing near offsets in

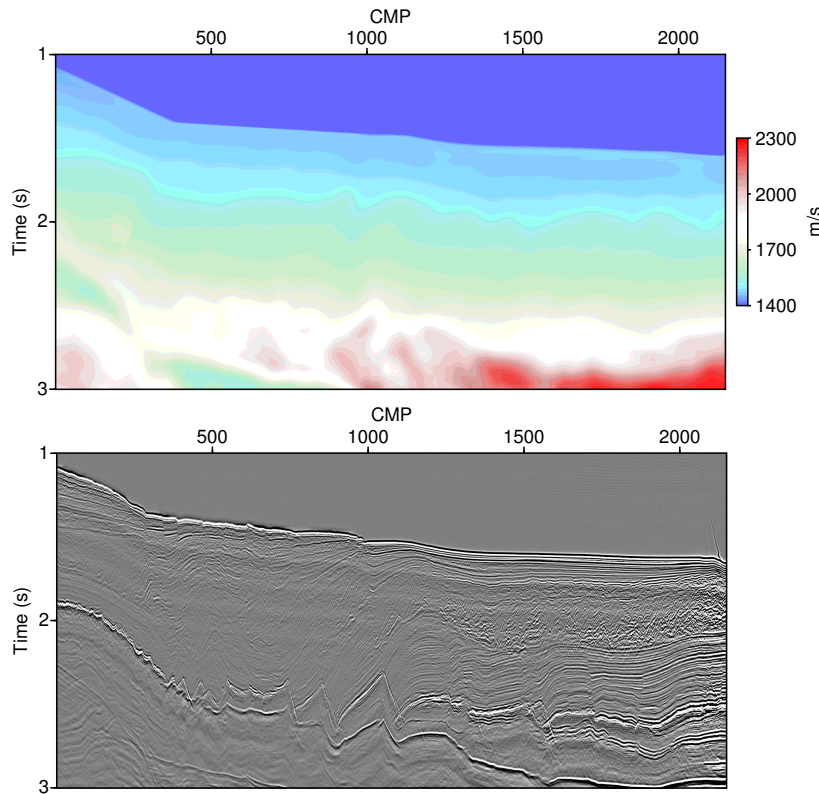


Figure 1: Updated velocity model (top) and prestack time migrated section (bottom).

data processing which usually results in a improper demultiple and defocused water-bottom reflection in migrated images. On of the expectation of the presented method is recovering of the amplitude for the water-bottom reflection.

Figure 4 shows on the left the first migrated image and on the right the second image. It displays a close up near to a complex salt intrusion which almost reaches the water bottom causing a complex fault structures in the shallow part of the sections. Instead of applying an $i\omega$ filter after de/migration we applied a low-cut filter to both images prior the inverse Hessian estimation.

Figure 5 shows result of migration on the left and migration deconvolution on the right. We observe a noticeable mitigation of migration swings, particularly for the salt flank, and the resolution enhancement. In shallow-water area we also observe wavelet recovery of the water-bottom reflection after migration deconvolution. On the contrary, the water bottom reflection after migration is widely destroyed. Several events in the middle of the section (between 1-1.5 second) are recognisable as reflections in the deconvolved image while they appear as migration swings in the migrated image. These events however are internal multiple reflections which once again indicate the difficulty of the demultiple in the shallow marine acquisition, particularly where a diapir is located very close to the water bottom. Nevertheless, these multiple reflections can be used in our case to track the flank of the diapir in the velocity model by their back projection. We also note some limitations of the current matching filter implementation (depicted with red arrows). It appears that the used filter length was not sufficient for very low frequency reflections. A cascaded filter application with different filter length however seems to resolve this issue.

CONCLUSIONS

We presented a time imaging method based on a migration/demigration loop. The method comprises an automatic model building (time-migration velocities) and an update of the migrated image (reflectivity).

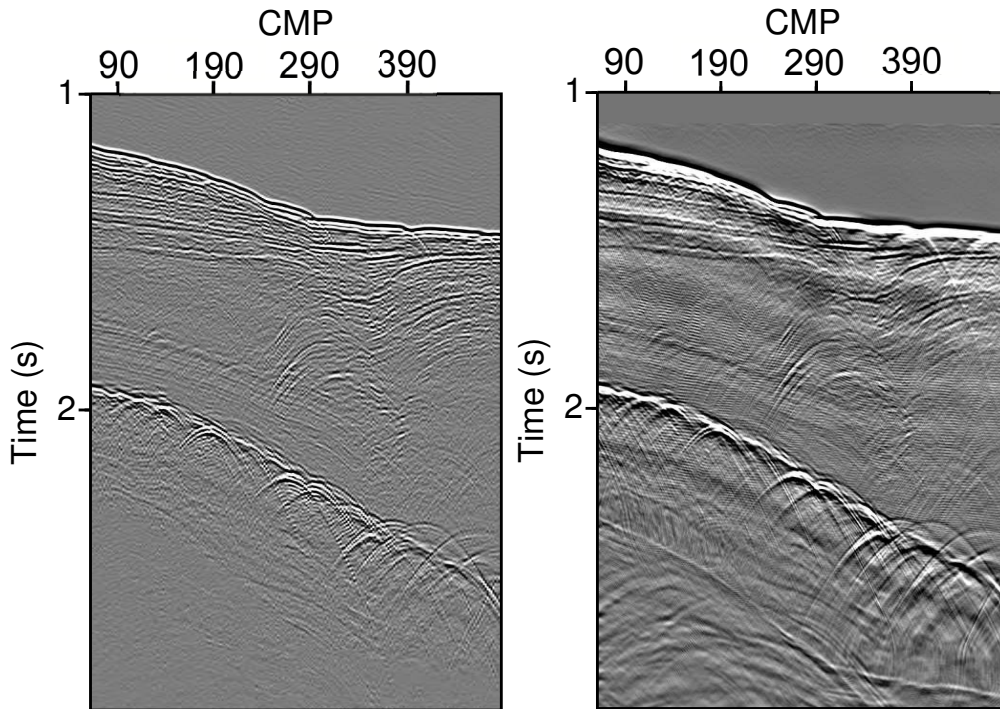


Figure 2: Close up of common offset sections: original data (left) and demigrated data (right). We did not apply an $-i\omega$ filter after demigration here, therefore low frequency noise is clearly to recognise in the demigrated result. Usually, a leaky integration is applied to (time) demigrated sections.

The basis for the forward (modelling) and backward (migration) transformation between different domains is a re-parametrized implicit CRS operator, which we rewrite in the operator apex coordinates. Exploiting the implicit CRS operator also allows us to use kinematic wavefield attributes extracted during the high-resolution CRS-parameter analysis.

The benefits of the migration/demigration loop are that seismic data becomes regularised and enhanced. Moreover, the conflicting dips are naturally handled correctly as migration repositions/removes the dips and the subsequently applied demigration restores them. To further improve the velocity model, we propose to incorporate the coherence section provided by the migration operator into the model building process. A certain coherence threshold is selected and serves as a mask to filter the velocity model which is subsequently interpolated and smoothed. The presented method enhances velocity models not only in areas assigned to the prominent reflections but also in vicinities of weaker diffractions.

The duality of migration/demigration operators allows to formulate time migration as a least-squares problem. We directly approximate the inverse of the Hessian by nonstationary matching filters. The inverse of the Hessian is then convolved with the migrated image which yields a deconvolved migrated image, i.e., the desired least-squares estimate of the reflectivity model. We almost do not make any model assumption and perform our velocity model building and migrated-image update in a data-driven fashion. Therefore, a minimal user interaction is required to carry out both the model and image update.

Applications to complex field data examples including shallow-water, complex salt intrusions and diagonal faulting, show very promising results for both building of a suitably smooth velocity model and migrated image enhancement.

ACKNOWLEDGMENTS

We thank the members of the Applied Seismic Group Hamburg for continuous discussions, especially Jan Walda for providing global optimised attributes for the calculation of the velocities. Further thanks goes to TGS and RWE Dea for providing the data sets. This work was partly supported by the sponsors of the

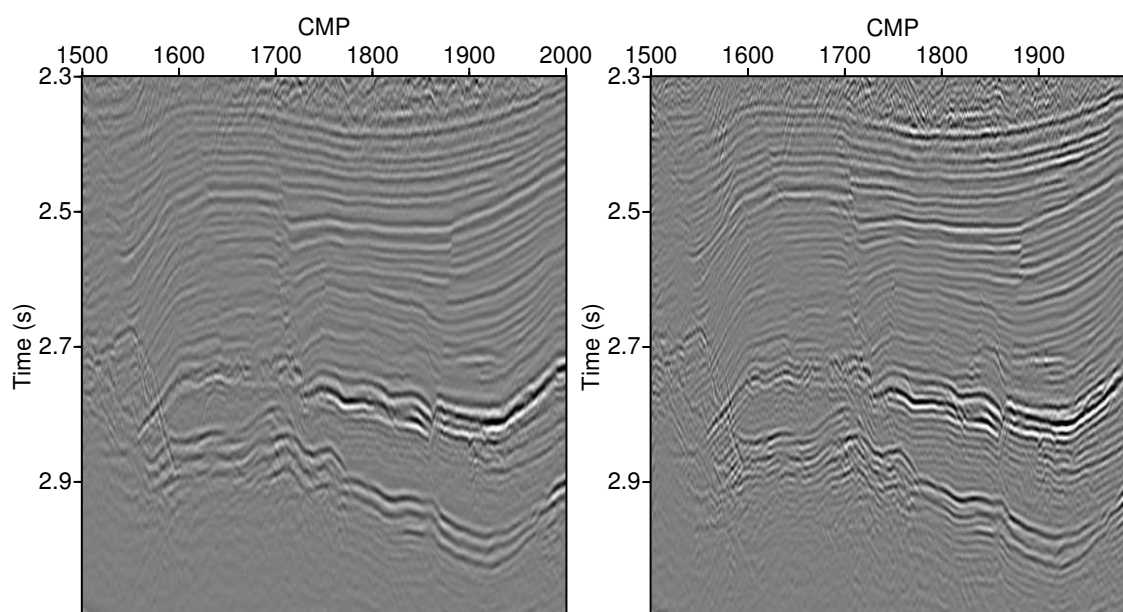


Figure 3: Close up of migrated sections. Left: conventional migration result, i.e., the first image in our deconvolution flow. Right: updated migration result, i.e., the first image convolved with the inverse of the Hessian.

Wave Inversion Technology (WIT) Consortium.

REFERENCES

- Bobsin, M. (2014). Time Migration applying the i-CRS Operator. Master's thesis, University Hamburg.
- Claerbout, J., Green, C., and Green, I. (1996). *Imaging the Earth's Interior*. Free Software Foundation.
- Claerbout, J. F. (2004). *Geophysical image estimation by examples*. Free Software Foundation.
- Dell, S., Gajewski, D., and Vanelle, C. (2012). Prestack time migration by common-migrated-reflector-element stacking. *Geophysics*, 77(3):S73–S82.
- Gloekner, M., Schwarz, B., Vanelle, C., and Gajewski, D. (2016). Kinematic time demigration with an automatically generated velocity model. *78th EAGE Conference and Exhibition*. Expanded Abstract.
- Guïtton, A. (2004). Amplitude and kinematic corrections of migrated images for nonunitary imaging operators. *Geophysics*, 69(4):1017–1024.
- Hertweck, T., Jäger, C., Goertz, A., and Schleicher, J. (2003). Aperture effects in 2.5D Kirchhoff migration: A geometrical explanation. *Geophysics*, 68:1673–1684.
- Hu, J., Schuster, G. T., and Valasek, P. (2001). Poststack migration deconvolution. *Geophysics*, 66:939–952.
- Hubral, P. (1983). Computing true amplitude reflections in a laterally inhomogeneous earth. *Geophysics*, 48:1051–1062.
- Hubral, P., Schleicher, J., and Tygel, M. (1996). A unified approach to 3-D seismic reflection imaging, Part I: Basic concepts. *Geophysics*, 61(3):742–758.

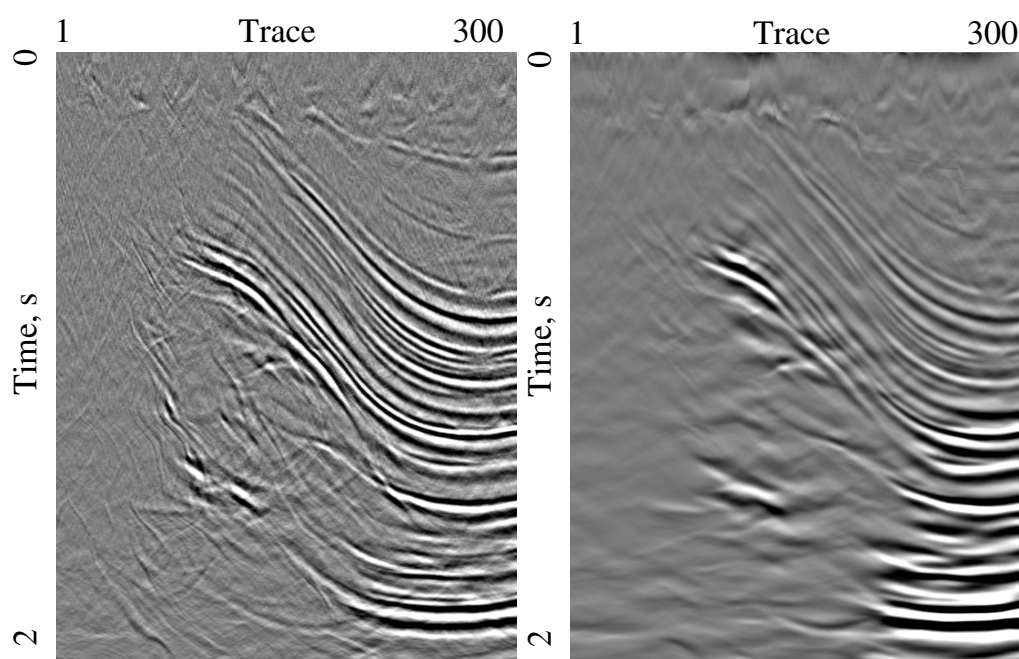


Figure 4: Migrated m_1 (left) and second image m_2 (right): close up. A section part close to the salt diapir. Instead of applying an $i\omega$ filter after de/migration we applied a low-cut filter to both images prior the inverse Hessian estimation.

Hübscher, C. and Netzeband, G. (2007). Evolution of a young salt giant: The example of the Messinian evaporites in the Levantine Basin. In: Wallner, M., Lux, K.-H., Minkley, W., Hardy, Jr., H.R. (Eds.) *The Mechanical behaviour of Salt - Understanding of THMC Processes in Salt*, pages 175–184.

Iversen, E., Tygel, M., Ursin, B., and de Hoop, M. (2012). Kinematic time migration and demigration of reflections in pre-stack seismic data. *Geophysical Journal International*, 189:1635–1666.

Jäger, R., Mann, J., Höcht, G., and Hubral, P. (2001). Common-reflection-surface stack: Image and attributes. *Geophysics*, 66:97–109.

Lambaré, G., Virieux, J., Madariaga, R., and Jin, S. (1992). Iterative asymptotic inversion in the acoustic approximation. *Geophysics*, 57:1138–1154.

Netzeband, G., Gohl, K., Håjbscher, C., Ben-Avraham, Z., Dehgahni, A., Gajewski, D., and Liersch, P. (2006). The Levantine Basin - crustal structure and origin Messinian evaporites in the Levantine Basin. *Tectonophysics*, 418:178–188.

Schwarz, B., Vanelle, C., Gajewski, D., and Kashtan, B. (2014). Curvatures and inhomogeneities: An improved common-reflection-surface approach. *Geophysics*, 79(5):S231–S240.

Tygel, M., Schleicher, J., and Hubral, P. (1996). A unified approach to 3-D seismic reflection imaging, Part II: Theory. *Geophysics*, 61(3):759–775.

Walda, J., Schwarz, B., and Gajewski, D. (2017). A competitive comparison of multiparameter stacking operators. *Geophysics*, 82(4):V275–V283.

Yilmaz, O. and Claerbout, J. F. (1980). Prestack partial migration. *Geophysics*, 45:1753–1779.

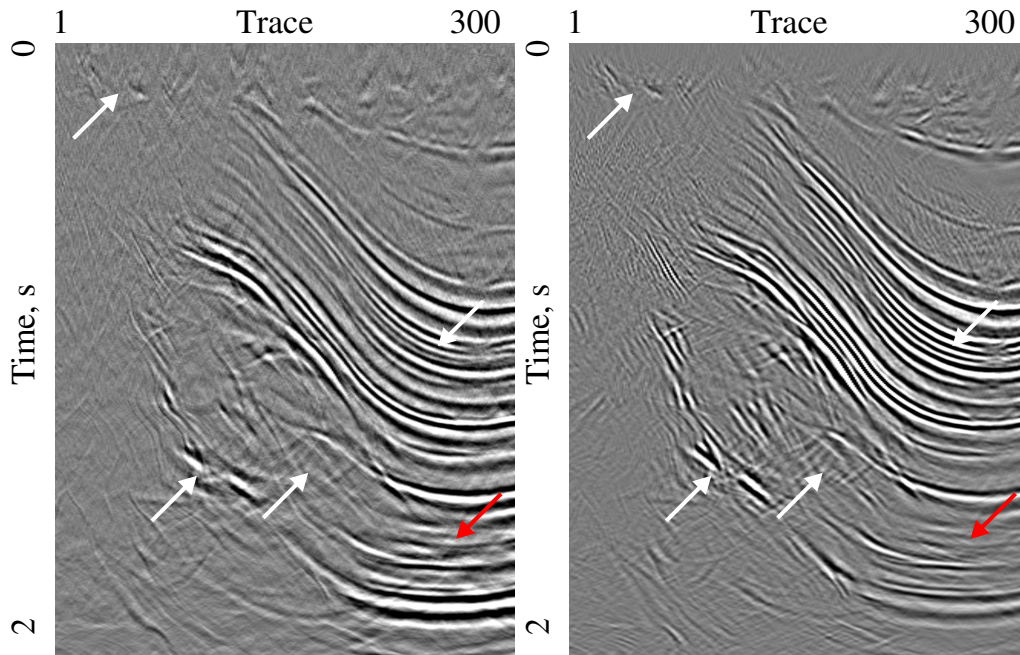


Figure 5: Result of migration (left) and migration deconvolution (right). We observe a noticeable mitigation of migration swings, particularly for the salt flank, and the resolution enhancement. We also note some limitations of the current matching filter implementation. It appears that the used filter length was not sufficient for very low frequency reflections. A cascaded filter application with different filter length however seems to resolve this issue.

APPENDIX A

In this appendix we investigate the proposed migration/demigration operators. In the mathematical sense, every adjoint operator (in our case migration operator) is defined by a dot product test (Claerbout, 2004). For the dot-product test, we first fill two vectors x and y with random numbers. Then we compute the vector $\hat{y} = Lx$ where L represents our modelling (demigration) operator given by Equation 3. We also compute $\hat{x} = L'y$ where L represents our inverse (migration) operator given by Equation 1.

$$y'(Lx) = y'\hat{y} = \hat{x}'x = (L'y)'x \quad (7)$$

The most left and right sides of the equation should be computationally equal up to a small tolerance error only if the adjoint operator L' is indeed an adjoint to the modelling operator L .